Electronic States of Al_3As_2, $Al_3As_2^-$, $Al_3As_2^+$, Al_2As_3, $Al_2As_3^-$, and $Al_2As_3^+$

Ping Yi Feng,[†,‡] Dingguo Dai,[‡] and K. Balasubramanian*[,‡]

State Key Laboratory of Functional Materials for Informatics, Shanghai Institute of Metallurgy, Academia Sinica, Shanghai 200050, China, and Department of Chemistry and Biochemistry, Arizona State University, Tempe, Arizona 85287-1604

Received: August 30, 1999; In Final Form: November 1, 1999

We have computed the optimized geometries and energy separations for the electronic states of Al_3As_2, Al_2As_3, and their positive and negative ions using complete active-space MCSCF (CASSCF) followed by multireference singles + doubles configuration interaction (MRSDCI) calculations which included up to 3.9 million configurations. The $^2A_1(C_{2v})$ state is the lowest electronic state of Al_3As_2 among seven states with distorted trigonal bipyramid structures. The $^2A_1$ state and another distorted $^2B_1(C_{2v})$ state are formed from the undistorted $^2E'$ and $^2E''(D_{3h})$ states, respectively, as a consequence of Jahn−Teller effect. The $^2A_2''(D_{3h})$ state is found to be the ground state of Al_2As_3 with an undistorted trigonal bipyramid structure (D_{3h}). Four electronic states of $Al_3As_2^+$ and $Al_2As_3^+$ were computed and their ground states are undistorted $^3A_2'$ and $^1A_1'(D_{3h})$ states for $Al_3As_2^+$ and $Al_2As_3^+$, respectively. The $^1A_1'(D_{3h})$ state is the ground state for both $Al_3As_2^-$ and $Al_2As_3^-$. The atomization energies, adiabatic ionization potentials, and other properties for the electronic states of Al_3As_2 and Al_2As_3 and a comparison with the Ga analogues are provided. The Al_3As_2 cluster is shown to differ from Ga_3As_2 in some states due to a greater charge transfer from Al(3s) to As(4p) in Al_3As_2.

I. Introduction

Spectroscopic and geometrical properties of group III−V (group 13−15) and other related mixed main group clusters[1−32] have been investigated intensely not only due to their intrinsic merit but also due to their technological importance. The III−V materials find applications in the emerging semiconductor technology of fast devices and light-emitting diodes. It is of great experimental and theoretical interest to study how the clusters evolve as a function of their sizes to the bulk, as smaller clusters exhibit dramatic variations in their properties and relative abundance compared to larger clusters.

Early interest in group III−V clusters arose from the pioneering work of Smalley and co-workers[1] on Ga_xAs_y; they showed that while the relative abundance of larger clusters followed a binomial distribution, the abundance of smaller clusters deviated strongly from the anticipated binomial distribution. Subsequently, driven by the technological importance of these species and the availability of experimental techniques to generate these species, such as the supersonic jet expansion method, spectroscopic studies of many III−V clusters have been carried out. In the supersonic jet method, a source material of the III−V compound, such as a foil of the material, is laser-evaporated. The vapor thus formed is passed through a supersonic nozzle, which results in cooling and formation of copious amounts of clusters of various sizes.[6] The clusters can be mass-analyzed and a variety of spectroscopic techniques could then be utilized to probe the low-lying electronic states of these clusters as a function of their sizes.

Negative ion photoelectron spectroscopy is a powerful method to probe the ground and excited electronic states of the neutral clusters since mass analysis of the generated anionic clusters would confirm the cluster sizes unequivocally. In addition, the technique has reasonable spectral resolution. Newmark and co-workers[4−5,7,8] have studied a number of III−V clusters, especially Ga_xP_y, In_xP_y, Ga_xAs_y, etc. Experimental studies of other III−V clusters such as Al_xP_y, Al_xAs_y, etc., are in progress.[15] These experimental results have revealed several fascinating trends for the measured electron affinities and other properties of the low-lying electronic states of the neutral clusters. The experimental studies have yielded electron affinities, term values, and vibrational frequencies of the neutral and anionic clusters. In a recent experimental study, Taylor et al.[15] have demonstrated that vibrationally resolved anion photoelectron spectra of III−V clusters, such as GaP_2^- and $Ga_2P_3^-$ anions, could be obtained, thus providing more accurate term values, electron affinities, and vibrational frequencies of such species.

Weltner and co-workers[11−13] have used a matrix-isolation technique to study a few group III−V clusters. Subsequently, ESR or far-IR spectroscopic methods have been used to probe the ground states of the matrix-isolated clusters. On the basis of the hyperfine patterns, the spin multiplicities, and the grometries of the ground states of these species can be deduced. These authors[11] have obtained the far-infrared spectra of Ga/P, Ga/As, and Ga/Sb clusters in rare gas matrices at 4 K. Few vibrational spectroscopic studies of the group III−V clusters have been performed; at present such studies are restricted to GaP, GaAs, and GaSb in a rare gas matrix. As noted before, Taylor et al.[15] have reported vibrationally resolved spectra on larger clusters including pentamers.

Van Zee et al.[12] have studied a pentamer cluster related to the title cluster of our current study. They have obtained the hyperfine interaction and structure of Ga_2As_3 using the matrix-isolation method. These authors have employed a laser vaporization technique for GaAs crystals followed by aggregation at a relatively high pressure of Ar/Kr prior to condensation of the matrices at 4 K, which yielded a pentameric Ga_2As_3 cluster.

* To whom correspondence should be addressed. E-mail: kbalu@asu.edu.
† Shanghai Institute of Metallurgy.
‡ Arizona State University.

10.1021/jp993074+ CCC: $19.00
Published on Web 12/16/1999

Electron spin resonance revealed a doublet ground state with a hyperfine pattern that suggested a trigonal bipyramid structure (tbp) in a probable ground state of $^2A_2''$.

Duncan and co-workers[18−20] have studied several mixed main group cluster cations, such as $In_xSb_y^+$, using the photoionization and photodissociation techniques. Such studies have revealed interesting information on the photofragmentation patterns as well as spectroscopic data on the excited states of their cations. The current theoretical study is aimed at the excited states of not only neutral clusters but also the cations.

Stimulated by experimental studies on these clusters, several theoretical studies were directed toward the geometrical and electronic properties of group III−V clusters.[14−24] These studies have varied from molecular dynamics methods to relativistic ab initio CASSCF and MRSDCI techniques. However, to the best of the present authors' knowledge, the low-lying electronic states of the clusters containing Al and As have not been studied before at the level of theory considered here. The present paper deals with the low-lying electronic states of Al_3As_2 and Al_2As_3 and their positive and negative ions using high-level relativistic ab initio CASSCF and MRSDCI techniques that included up to 3.91 million configurations.

II. Method of Computations

In the present study, we use a relativistic CASSCF/MRSDCI method to compute the electronic properties of the neutral, cationic, and anionic clusters. Geometries were fully optimized at the CASSCF level and the MRSDCI technique was employed for further geometry optimization and term energies. We employed relativistic effective core potentials(RECPs) that retained the outer $3s^23p^1$and $4s^24p^3$ shells of the Al and As atoms explicitly in the valence space, replacing the remaining electrons by RECPs. The RECPs together with the valence Gaussian basis sets were taken from ref 33. These basis sets were augmented with a set of 3d polarization functions with exponent $\alpha_d = 0.3084$ for Al and $\alpha_d = 0.22$ for As, respectively.

The CASSCF technique was used to generate the molecular orbitals for higher-order MRSDCI calculations. In the CASSCF calculations, five s orbitals of Al and As were kept in the core in that excitations were not allowed from these orbitals, but they were allowed to relax as a function of geometries. The computations were carried out in the C_{2v} group, although many of the relevant electronic states have D_{3h} symmetries. The CASSCF wave function that included i a_1, j b_2, k b_1, l a_2 orbitals in the active space is labeled *ijkl*-CAS. On the basis of the results of several trial computations and the previous work on other isovalent pentameric clusters,[31] we adopted a 3232-CAS method for the Al_3As_2, Al_2As_3, and their ions. Thus, nine active electrons for Al_3As_2 (eight electrons for $Al_3As_2^+$ and 10 electrons for $Al_3As_2^-$) and 11 active electrons for Al_2As_3 (10 electrons for $Al_2As_3^+$ and 12 electrons for $Al_2As_3^-$) were distributed in all possible ways among the chosen set of active orbitals in the CASSCF.

It is anticipated that some of the electronic states with the D_{3h} geometry would be subjected to Jahn−Teller distortion, if the electronic states under consideration were E′ or E″ states. This is consistent with a previous study on the electronic states of Ga_3P_2 and $Ga_2P_3$31, which has revealed two distorted states with C_{2v} symmetries, although the extent of distortion was rather small. Consequently, we optimized the geometries using a quasi Newton−Raphson technique at the CASSCF level of theory. For this purpose, the GAMESS[34] molecular computational package was employed. Two distorted electronic states of the neutral clusters, namely $^2A_1$, $^2B_1$(C_{2v}) of Al_3As_2 and $^2A_2$, $^2A_1$-(C_{2v}) for Al_2As_3 were found to arise from Jahn−Teller distortion of the $^2E'$ and $^2E''$ states, respectively. However, the ground states of the anion and cation are found to be undistorted. The geometries of all possible low-lying doublet and quartet electronic states for Al_3As_2 and the doublet states of Al_2As_3 were searched and optimized.

We have also considered an isomer of Al_3As_2 in which the As atoms are in tetra coordination. One may visualize this as an isomer of the distorted tbp structure considered above, but one of the axial As atom switched to the equatorial position such that there would be two As and an Al at the equatorial position and two Al atoms at the axial sites. However, geometry optimization of such a structure would rearrange the structure so that the Al atoms move away from the center of the triangle above the plane so as to form a direct As−Al−As bridge. This results in a capped rhombus structure in which two As and two Al atoms form a planar rhombus structure, wherein the As−As bond is the shorter diagonal of the rhombus, the Al−Al bond is the longer diagonal, and the four equal sides are the Al−As bonds. The third Al atom is above the plane of the rhombus at the middle of the As−As bond so as to form a As−Al−As bridge with Al−As bond lengths being the same as the other four Al−As bonds in the rhombus structure. The resulting structure exhibits C_{2v} symmetry. We considered two low-lying states ($^2A_1$ and $^2B_1$) for this structure, and the geometries were optimized at the CASSCF level. Among the two states, the $^2B_1$ state was found to be lower and thus it was considered for higher level of theory. However, it is clear that this structure is not a viable candidate for Al_2As_3 since the As atoms tend to cling together and it would take significant energy to break the As−As bonds, while in the case of Al_3As_2, the Al−Al bonds are weaker than the Al−As bonds.

The multireference singles + doubles configuration interaction (MRSDCI) calculations were carried out following the CASSCF computations to introduce higher-order electron correlation effects. All configurations in the CASSCF with absolute coefficients larger than 0.07 were included as reference configurations in the MRSDCI computations. This created up to 3 909 883 configuration spin function (CSFs) in the MRSDCI computations. Furthermore, a multireference Davidson correction technique for uncoupled quadruple clusters to the MRSDCI energy was invoked and the resulting energy separation was labeled as MRSDCI+Q, which is considered to be a full-CI estimate.

As noted earlier, it would be useful to compute the ground and excited electronic states of the $Al_3As_2^+$ and $Al_2As_3^+$ ions, as the results of such computations would be useful in photoionization studies of these species. Likewise, anions of these species are of interest in the anion photoelectron spectroscopic studies carried out by Neumark and co-workers.[15,16] Consequently, computations on the $Al_3As_2^-$ and $Al_2As_3^-$ anions as well as four low-lying electronic states of $Al_3As_2^+$ and $Al_2As_3^+$ were carried out. Furthermore, the atomization energies to dissociate the Al_3As_2 and Al_2As_3 clusters into aluminum (^2P) and arsenic atoms (^4S) were computed as supermolecular calculations.

The CASSCF/MRSDCI calculations were made using a version of ALCHEMY II codes[36] modified by one of the authors[35] to include relativistic ECPs (RECPs).

III. Results and Discussion

A. Electronic States of Al_3As_2, $Al_3As_2^+$, and $Al_3As_2^-$. The first part of Table 1 shows the optimized geometries, energy separations, and dipole moments for two of the lowest Jahn−

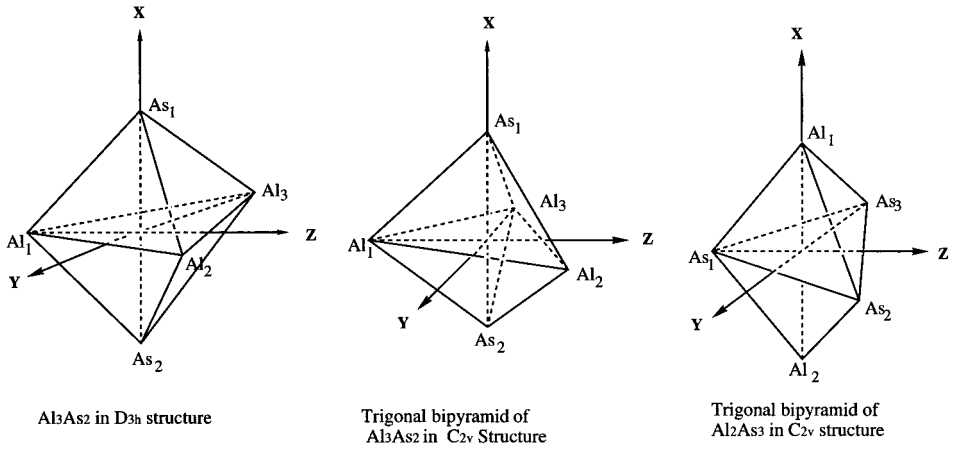

Figure 1. Geometries of regular trigonal bipyramid (tbp), distorted tbp structures of Al_3As_2, and the regular tbp structure of Al_2As_3.

TABLE 1: Geometries and Energy Separations for the Electronic States of Al_3As_2 with Distorted Tbp and Capped Rhombus and Al_2As_3 with Distorted Tbp Structures

		distorted tbp states (C_{2v})		capped rhombus states (C_{2v})	
species		$^2A_1$	$^2B_1$	$^2B_1$	$^2A_1$
Al_3As_2	$Al_2-Al_1-Al_3$ (deg)	69.5	71.7	45.0	45.0
	$As_1-Al_1-As_2$ (deg)	67.9	51.1	53.0	60.5
	$As_1-Al_2-As_2$ (deg)	59.9	53.8	53.0	60.5
	Al_1-Al_2 (Å)	3.641	3.902	4.833	4.469
	Al_2-Al_3 (Å)	4.153	4.568	3.417	3.160
	Al_1-As_1 (Å)	2.384	2.793	2.700	2.587
	Al_2-As_1 (Å)	2.667	2.661	2.700	2.587
	As_1-As_2 (Å)	2.663	2.410	2.409	2.607
	dipole moment (D)	−5.42	−1.29	−0.14(X)	
	E(CASSCF) (eV)	0.00	0.51	0.76	1.04
	E(MRSDCI) (eV)	0.00	0.63	0.46	
	E(MRSDCI+Q) (eV)	0.00	0.58	0.54	

		distorted tbp states (C_{2v})	
species		$^2A_2$	$^2A_1$
Al_2As_3	$As_2-As_1-As_3$ (deg)	55.6	49.6
	$Al_1-As_1-Al_2$ (deg)	136.0	90.7
	$Al_1-As_2-Al_2$ (deg)	110.8	88.6
	As_1-As_2 (Å)	2.485	3.184
	As_2-As_3 (Å)	2.319	2.672
	As_1-Al_1 (Å)	2.624	2.442
	As_2-Al_1 (Å)	2.956	2.487
	Al_1-Al_2 (Å)	4.865	3.475
	dipole moment (D)	−0.63	−0.21
	E(CASSCF) (eV)	0.41	1.05
	E(MRSDCI) (eV)	0.69	0.94
	E(MRSDCI+Q) (eV)	0.80	0.92

Teller distorted electronic states of Al_3As_2, namely $^2A_1$ and $^2B_1$-(C_{2v}), and also two states for the isomer with capped rhombus structure described before. Figure 1 illustrates the actual locations for the atoms. Table 2 exhibits all undistorted doublet and quartet electronic states of Al_3As_2 with their ideal trigonal bipyramid geometries (D_{3h}), and their energy separations. As can be seen from Table 2, the first two low-lying electronic states of Al_3As_2 with regular D_{3h} structures are the $^2E'$ and $^2E''$ states which would be subjected to Jahn−Teller distortion. Among the undistorted D_{3h} states, the $^2E'$ state is the lowest in energy. The $^2E''$ state is 0.35 eV above the $^2E'$ state, and all of the quartet states are higher at both CASSCF and MRSDCI levels of theory. The geometries of the distorted $^2A_1$ and $^2B_1$-(C_{2v}) states of Al_3As_2 can be visualized as the derivatives of the $^2E'$ and $^2E''$ states by Jahn−Teller effect. Consequently, the distorted $^2A_1$ and $^2B_1$(C_{2v}) states of Al_3As_2 in Table 1 are the lowest C_{2v} Jahn−Teller components arising from the $^2E'$ and $^2E''$ states, respectively. Consequently, the $^2A_1$(C_{2v}) state is 0.27 eV lower than the corresponding $^2E'$(D_{3h}) state, while the $^2B_1$-(C_{2v}) state is only 0.06 eV lower than the $^2E''$(D_{3h}) state at the MRSDCI level of theory. Thus, the Jahn−Teller stabilization energy is rather small, especially for the $^2E''$(D_{3h}) state. This is further confirmed by a small geometry change between the distorted and undistorted structures. At all levels of theory, the $^2A_1$(C_{2v}) state prevails as the ground state of Al_3As_2, while the $^2B_1$(C_{2v}) state is 0.56 eV above the $^2A_1$ state at the MRSDCI level.

As seen from Table 2, the three Al atoms form an equilateral triangular base for the $^2E'$(D_{3h}) state. The three Al atoms depart from the equilateral triangular position in the $^2A_1$(C_{2v}) state due to Jahn−Teller distortion, resulting in two contracted Al_1-Al_2 and Al_1-Al_3 (3.641 Å) bonds, and an elongated Al_2-Al_3 (4.153 Å) bond. However, the average Al−Al bond length of 3.812 Å for the $^2A_1$(C_{2v}) state is close to the Al−Al distance (3.748 Å) in the $^2E'$(D_{3h}) state. The As_1-As_2 bond length in the $^2A_1$(C_{2v}) state is 2.663 Å, which is quite comparable to 2.704 Å in the $^2E'$(D_{3h}) state (see, Tables 1 and 2). Likewise, the average Al−Al bond length of the three Al−Al bonds, namely Al_1-Al_2, Al_1-Al_3 (3.902 Å) and Al_2-Al_3 (4.568 Å) in the $^2B_1$(C_{2v}) state is 4.124 Å, which is near the Al−Al bond length (4.142 Å) in the $^2E''$(D_{3h}) state. On the other hand, the As_1-As_2 bond length of 2.410 Å in the $^2B_1$(C_{2v}) state is close to 2.469 Å in the $^2E'$-(D_{3h}) state. These features suggest that the Al atoms move from their ideal equilateral triangular locations in the D_{3h} structures of Al_3As_2 due to Jahn−Teller effect, but the As atoms do not change their axial positions substantially.

The As−As bond length of the As_2 dimer is 2.164 Å in the $^1\Sigma_g^+$ ground state.[37] The As−As bond distances in the first two low-lying electronic states of Al_3As_2 are near 2.50 Å, similar to those in the excited states of As_2. However, the Al−Al distances exhibit a different behavior. The Al_1-Al_2 and Al_2-Al_3 bond lengths in the $^2A_1$ ground state of Al_3 are 2.521 and 2.559 Å,[38] respectively. These values are much shorter than the Al−Al bond lengths (3.2−4.6 Å) in Al_3As_2. Evidently the interactions among the three Al atoms in Al_3As_2 are weakened by the bonding between Al and As atoms in Al_3As_2.

It is noticeable that the $As_1-Al_1-As_2$ and $As_1-Al_2-As_2$ bond angles in the $^2B_1$ state (51.1° and 53.8°, respectively) are considerably smaller than the corresponding values of 67.9° and 59.9° in the $^2A_1$ state, respectively. This suggests a stronger As−As bonding in the $^2B_1$ state compared to that in $^2A_1$. This is consistent with the fact that the As−As bond length in the $^2B_1$ state is 2.410 Å which is shorter than 2.663 Å for $^2A_1$. However, the Al_1-As_1 bond length is 2.384 Å, while the Al_1-

TABLE 2: Electronic States of Al_3As_2, Al_2As_3 and Their Ions: D_{3h} Tbp Structures

	state		MRSDCI			
species	C_{2v}	D_{3h}	Al−Al (Å)	Al−As (Å)	As −As (Å)	E (eV)[a]
Al_3As_2	$^2A_1$, $^2B_2$	$^2E'$	3.748	2.552	2.704	0.27 (0.22)
	$^2B_1$, $^2A_2$	$^2E''$	4.142	2.691	2.469	0.61 (0.58)
	$^4A_2$	$^4A_1''$	3.205	2.499	3.360	0.73 (0.58)
	$^4B_1$, $^4A_2$	$^4E''$	3.193	2.517	3.427	1.48 (1.45)
	$^4A_1$, $^4B_2$	$^4E'$	3.549	2.611	3.236	2.35 (2.16)
	$Al_3(^2A_1) + 2As(^4S)$					5.58 (5.69)
	$3Al(^2P) + 2As(^4S)$					8.90 (9.27)
$Al_3As_2^+$	$^3B_2$	$^3A_2'$	3.748	2.552	2.704	6.84 (6.77)
	$^1A_1$, $^1B_2$	$^1E'$	3.748	2.552	2.704	7.02 (7.11)
	$^3B_1$, $^3A_2$	$^3E''$	3.748	2.552	2.704	8.09 (8.03)
	$^1B_1$, $^1A_2$	$^1E''$	3.748	2.552	2.704	8.74 (8.62)
$Al_3As_2^-$	$^1A_1$	$^1A_1'$	3.839	2.574	2.616	−2.33 (−2.37)
	state		MRSDCI			
species	C_{2v}	D_{3h}	As−As (Å)	As−Al (Å)	Al−Al (Å)	E (eV)[a]
Al_2As_3	$^2B_1$	$^2A_2''$	2.556	2.560	4.184	0.00 (0.00)
	$^2A_2$, $^2B_1$	$^2E''$	2.457	2.800	4.828	1.02 (1.01)
	$^2A_1$, $^2B_2$	$^2E'$	2.950	2.456	3.539	1.49 (1.45)
	$As_3(^2A_2) + 2Al(^2P)$					7.59 (7.71)
	$3As(^4S) + 2Al(^2P)$					12.77(13.12)
$Al_2As_3^+$	$^1A_1$	$^1A_1'$	2.556	2.560	4.184	6.61 (6.87)
	$^3B_1$	$^3A_2''$	2.556	2.560	4.184	7.66 (8.00)
	$^3B_2$, $^3A_1$	$^3E'$	2.556	2.560	4.184	7.96 (8.29)
	$^1B_1$	$^1A_2''$	2.556	2.560	4.184	8.92 (8.93)
$Al_2As_3^-$	$^1A_1$	$^1A_1'$	2.495	2.658	4.468	−2.05 (−1.94)

[a] The values in the parentheses are the Davidson corrected energies.

Al_2 and Al_2-Al_3 bond distances in the $^2A_1$ state are 3.641 and 4.153 Å, respectively. All these distances are shorter than their corresponding values of 2.793 (Al_1-As_1), 3.902 (Al_1-Al_2), and 4.568 Å (Al_2-Al_3) in the $^2B_1$ state. The $^2A_1$ state remains as the ground state of Al_3As_2 at all levels of theory, while the $^2B_1$ state is 0.56 eV higher than the $^2A_1$ state at the MRSDCI level, suggesting that the interaction between the Al and As atoms has a greater influence on the term energies and geometries of the electronic states of Al_3As_2. Likewise, the $As_1-Al-As_2$ bond angle of the $^2E''$ state (54.6°) for the undistorted structure is smaller than the corresponding angle of 64.0° in the $^2E'$ state. This is caused by a shorter As−As bond length (2.469 Å) in the $^2E''$ state compared to the As−As bond (2.704 Å) in the $^2E'$ state. Thus, the As−As bonding in the $^2E''$ state is stronger than that in the $^2E'$ state. However, the $^2E'$ state is 0.35 eV lower than the $^2E''$ state because both Al−As and Al−Al bonds of $^2E'$ are stronger than those of $^2E''$. As seen from Table 2, all of the quartet states of the undistorted D_{3h} structure were also computed, but these states, namely $^4A_2''$, $^4E''$, and $^4E'$, are higher in energy than $^2E''$.

The capped rhombus structures shown in Table 1 for Al_3As_2 can be envisaged as derivatives from the Al_2As_2 molecule, which exhibits a rhombus ground state with the As−As bond being the shorter diagonal of the rhombus. The As−Al bonds are the four equal sides of the rhombus. The capped rhombus structure is derived from this by adding the third Al atom above the center of the As−As bond (As−As edge capping) such that the Al−As bond distances are the same as those of the four sides of the rhombus. As seen from Table 2, two low-lying electronic states arise from this isomer, the $^2B_1$ being the lower of the two. However, this state is 0.76 and 0.46 eV higher than the distorted tbp $^2A_1$ state at the CASSCF and MRSDCI levels, respectively. While it falls slightly below the distorted tbp $^2B_1$ state at the MRSDCI level, it is still higher than the distorted tbp $^2A_1$ state. The capped rhombus and distorted tbp structures are nearly degenerate for the $^2B_1$ state at the MRSDCI+Q level (Table 1). Hence this state should be considered as an excited isomer for Al_3As_2. It should be noted that the $^2B_1$ state with the capped rhombus structure is multireference in character in that three reference configurations have coefficients larger than 0.1 and 12 reference configurations have coefficients of 0.07 or more. This is reflected in the MRSDCI energy separation of this state, which is lower than the CASSCF energy separation.

The nature of bonding in the electronic states can be comprehended through the leading configurations, compositions of the orbitals, and the Mulliken populations. Table 3 shows the leading configurations for the electronic states of Al_3As_2 and its ions. The distorted electronic states of Al_3As_2 with C_{2v} geometries ($^2A_1$ and $^2B_1$) have ($1a_1^2 2a_1^2 3a_1^2 4a_1^2 1b_2^2 2b_2^2 1b_1^2 1a_2^2$) portion of the configuration in common for both states. Likewise, all of the undistorted electronic states with D_{3h} symmetries have ($1a_1'^2 2a_1'^2 1e'^4 1a_2''^2$) in common. We describe the compositions of the D_{3h} molecular orbitals (MOs), which can be correlated into the C_{2v} group. The $1a_1'$ ($1a_1$ in C_{2v}) orbital is predominantly $As_1(s) + As_2(s)$. The $2a_1'$ ($3a_1$ in C_{2v}) orbital is a bonding combination of $Al_1(s) + Al_2(s) + Al_3(s)$. The $3a_1'$ orbital ($4a_1$ in C_{2v}) is a bonding orbital composed of $As_1(p_x)$ and $As_2(p_x)$ in which the two As atoms furnish p orbitals overlapping with same sign along the x axis. The two degenerate components of the 1e′ orbital ($2a_1$ and $1b_2$ in C_{2v}) are $2Al_1(s) - [Al_2(s) + Al_3(s)]$ and $Al_2(s) - Al_3(s)$ linear combinations, respectively. The 2e′ orbital ($5a_1$ and $2b_2$ in C_{2v}) consists of two parts, viz., $[2Al_1(s) - [Al_2(s) + Al_3(s)]$ mixed with $[As_1(p_y) + As_2(p_y)]$ and $[Al_2(s) - Al_3(s)] + [As_1(p_z) + As_2(p_z)]$, respectively. Likewise, the two degenerate components of the 1e″ orbital ($2b_1$ and $1a_2$ in C_{2v}) are $[As_1(p_y) - As_2(p_y)]$ combined with $[2Al_1(p_x) - Al_2(p_x) - Al_3(p_x)]$ and $[As_1(p_z) - As_2(p_z)] + [Al_2(p_x) + Al_3(p_x)]$, respectively. The $1a_2''$ orbital ($1b_1$ in C_{2v}) is an antibonding $As_1(s) - As_2(s)$ orbital. The $2a_2''$ orbital ($3b_1$ in C_{2v}) is composed of $As_1(p_x) + As_2(p_x)$, which is antibonding with respect to the As atoms. As indicated in Table 3, the primary difference between the $^2A_1$ and $^2B_1$ states (C_{2v}) is in the electronic occupancies of the $5a_1$ and $2b_1$ orbitals. Both $5a_1$ and $2b_1$ orbitals exhibit antibonding character, the former relative

TABLE 3: Leading Configurations of the Electronic States of Al_3As_2, Al_2As_3, and Their Ions[a]

system	state C_{2v}	state D_{3h}	weight	configuration				
				$4a_1$	$5a_1$	$2b_2$	$2b_1$	$1a_2$
Al_3As_2	$^2A_1$		96	2	1	2	2	2
	$^2B_1$		96	2	2	2	1	2
				$3a_1'$	$2e'$	$1e''$	$2a_2''$	
	$^2A_1$, $^2B_2$	$^2E'$	96	2	3	4	0	
	$^2B_1$, $^2A_2$	$^2E''$	96	2	4	3	0	
	$^4A_2$	$^4A_1''$	96	2	2	4	1	
	$^4B_1$, $^4A_2$	$^4E''$	93	1	3	4	1	
	$^4B_2$,$^4A_1$	$^4E'$	94	2	3	3	1	
$Al_3As_2^+$	$^3B_2$	$^3A_2'$	96	2	2	4	0	
	$^1A_1$, $^1B_2$	$^1E'$	94	2	2	4	0	
	$^3B_1$, $^3A_2$	$^3E''$	96	2	3	3	0	
	$^1B_1$, $^1A_2$	$^1E''$	96	2	3	3	0	
$Al_3As_2^-$	$^1A_1$	$^1A_1'$	96	2	4	4	0	
				$4a_1$	$5a_1$	$2b_2$	$3b_1$	$1a_2$
Al_2As_3	$^2A_2$		96	2	2	2	2	1
	$^2B_1$		96	2	2	2	1	2
				$2a_1'$	$3a_1'$	$3e'$	$1e''$	$2a_2''$
	$^2B_1$	$^2A_2''$	96	2	2	0	4	1
	$^2A_2$, $^2B_1$	$^2E''$	96	2	2	0	3	2
	$^2B_2$, $^2A_1$	$^2E'$	95	2	2	1	4	0
$Al_2As_3^+$	$^1A_1$	$^1A_1'$	95	2	2	0	4	0
	$^3B_1$	$^3A_2''$	96	2	1	0	4	1
	$^3B_2$, $^3A_1$	$^3E'$	96	2	2	0	3	1
	$^1B_1$	$^1A_2''$	95	2	1	0	4	1
$Al_2As_3^-$	$^1A_1$	$^1A_1'$	96	2	2	0	4	2

[a] The $1a_1^2 2a_1^2 3a_1^2 1b_2^2 1b_1^2$ configuration part for Al_3As_2 (or $1a_1^2 2a_1^2 3a_1^2 1b_2^2 1b_1^2 2b_1^2$ for Al_2As_3) is same for all states in C_{2v} structure. Likewise, the $1a_1'^2 2a_1'^2 1e'^4 1a_2''^2$ configuration part for Al_3As_2 and its ions (or $1a_1'^2 1e'^4 2e'^4 1a_2''^2$ for Al_2As_3 and its ions) is common to all states in D_{3h} group.

to the Al atoms, and the latter relative to the As atoms. Consequently, a doubly occupied $2b_1$ orbital and a singly occupied $5a_1$ orbital in the $^2A_1$ state lead to longer As−As bond (2.663 Å) and relatively shorter Al_1-Al_2 (3.641 Å) and Al_2-Al_3 (4.153 Å) bonds compared to the corresponding parameters for the $^2B_1$ state. This in turn leads to larger $As_1-Al_1-As_2$ (67.9°) and $As_1-Al_2-As_2$ (59.9°) bond angles for the $^2A_1$ state. In contrast to the $^2A_1$ state, the $^2B_1$ state has a doubly occupied $5a_1$ orbital and a singly occupied $2b_1$ orbital leading to shorter As−As bond length (2.410 Å) and very acute $As_1-Al_1-As_2$ (51.1°) and $As_1-Al_2-As_2$ (53.8°) bond angles. However, in the $^2B_1$ state, both Al_1-Al_2 (3.902 Å) and Al_2-Al_3 (4.568 Å) bonds are longer than those in the $^2A_1$ state.

As expected, the main distinction between the $^2E'$ and $^2E''$ states of the undistorted Al_3As_2 cluster (D_{3h}) is in the electronic occupations of the 2e′ and 1e″ orbitals. Thus, the compositions of these two orbitals determine the geometries of the two states. As described above, the 2e′ orbital exhibits π bonds between the As atoms, while the 1e″ orbital is antibonding relative to the As atoms, but the interactions between the Al and As atoms are favorable. The 1e″ orbital of the $^2E'$ state is fully occupied, but the 2e′ orbital is only partially occupied leading to a longer As−As bond length (2.704 Å) but relatively shorter Al−As bond lengths (2.552 Å). On the other hand, the 2e′ orbital is fully occupied, but the 1e″ orbital is partially occupied in the $^2E''$ state. This leads to a shorter As−As bond length (2.469 Å) and relatively longer Al−As bonds (2.691 Å) in the $^2E''$ state.

All of the quartet electronic states have an occupied $2a_2''$ orbital, which consists of an antibonding interaction between the p_x orbitals of the two axial As atoms. Consequently, all of the quartet states are higher in energy.

As seen from Table 4, which displays the Mulliken populations of the electronic states of Al_3As_2, the total populations on the Al atoms are between 2.55 and 2.66, while the total As populations are about 5.51−5.61 for all of the states considered here. The depletion of the Al populations compared to the isolated Al atom and uniformly excessive As populations compared to the atomic As are attributed to charger transfers from the aluminum atoms to the As atoms leading to ionic Al^+ As^- bonding in the Al_3As_2 cluster. However, it is noted that

TABLE 4: Mulliken Populations for the Low-lying Electronic States of Al_3As_2, Al_2As_3, and Their Ions

						gross population								
	state		total			Al_1			Al_2			As		
system	C_{2v}	D_{3h}	Al_1	Al_2	As	s	p	d	s	p	d	s	p	d
Al_3As_2	$^2A_1$		2.547	2.623	5.605	1.233	1.209	0.105	1.822	0.731	0.070	1.815	3.615	0.175
	$^2B_1$		2.554	2.643	5.581	1.859	0.640	0.055	1.844	0.729	0.079	1.851	3.560	0.170
	$^2A_1$, $^2B_2$	$^2E'$	2.622		5.568	1.648	0.892	0.082				1.804	3.581	0.183
	$^2B_1$, $^2A_2$	$^2E''$	2.615		5.577	1.843	0.707	0.065				1.847	3.554	0.176
	$^4A_2$	$^4A_1''$	2.661		5.509	1.559	1.008	0.094				1.771	3.561	0.177
	$^4B_1$,$^4A_2$	$^4E''$	2.645		5.531	1.398	1.160	0.087				1.817	3.557	0.157
	$^4A_1$, $^4B_2$	$^4E'$	2.659		5.512	1.690	0.893	0.076				1.840	3.513	0.159
$Al_3As_2^+$	$^3B_2$	$^3A_2'$	2.355		5.466	1.539	0.737	0.079				1.800	3.473	0.193
	$^1A_1$, $^1B_2$	$^1E'$	2.349		5.477	1.487	0.783	0.079				1.806	3.480	0.191
	$^3B_1$, $^3A_2$	$^3E''$	2.444		5.334	1.727	0.637	0.080				1.807	3.318	0.209
	$^1B_1$, $^1A_2$	$^1E''$	2.437		5.345	1.647	0.707	0.083				1.805	3.325	0.215
$Al_3As_2^-$	$^1A_1$	$^1A_1'$	2.866		5.701	1.750	1.036	0.080				1.817	3.719	0.166

						gross population								
	state		total			As_1			As_2			Al		
system	C_{2v}	D_{3h}	As_1	As_2	Al	s	p	d	s	p	d	s	p	d
Al_2As_3	$^2A_2$		5.402	5.219	2.581	1.862	3.382	0.158	1.867	3.171	0.181	1.857	0.661	0.063
	$^2A_1$		5.307	5.303	2.545	1.871	3.329	0.107	1.888	3.294	0.121	1.278	1.137	0.130
	$^2B_1$	$^2A_2''$	5.277		2.586	1.876	3.247	0.154				1.537	0.939	0.110
	$^2A_2$, $^2B_1$	$^2E''$	5.273		2.591	1.878	3.223	0.172				1.855	0.671	0.065
	$^2B_2$, $^2A_1$	$^2E'$	5.321		2.520	1.886	3.315	0.120				1.256	1.128	0.136
$Al_2As_3^+$	$^1A_1$	$^1A_1'$	5.192		2.212	1.883	3.146	0.163				1.272	0.828	0.112
	$^3B_1$	$^3A_2''$	5.244		2.135	1.875	3.201	0.168				1.007	1.013	0.115
	$^3B_2$, $^3A_1$	$^3E''$	5.058		2.413	1.903	3.004	0.151				1.608	0.698	0.106
	$^1B_1$	$^1A_2''$	5.061		2.410	1.894	3.015	0.152				1.543	0.755	0.112
$Al_2As_3^-$	$^1A_1$	$^1A_1'$	5.424		2.864	1.853	3.401	0.170				1.739	1.034	0.091

both Al(s) and As(s) populations of all the electronic states are smaller than 2.0, implying small hybridization. Thus, most of the charge transferred from the Al atoms is mainly received by the As(p) orbitals.

The $^2A_1(C_{2v})$ ground state of Al_3As_2 is composed of Al_1-($s^{1.233}p^{1.209}$), Al_2($s^{1.822}p^{0.731}$), and As($s^{1.815}p^{3.615}$) Mulliken populations, while the corresponding populations for the $^2B_1(C_{2v})$ state are Al_1 ($s^{1.859}p^{0.640}$), Al_2($s^{1.844}p^{0.729}$), and As($s^{1.851}p^{3.560}$), where we have omitted the d populations as they are <0.21. The primary difference in the populations between these two states is in the s and p populations of the Al_1 atom. This is a consequence of the various electronic occupancies for the $5a_1$ and $2b_1$ orbitals. The $5a_1$ orbital has Al_1(s) as its principal component, while the $2b_1$ orbital contains a large contribution from Al(p_x). Since the $2b_1$ orbital is fully occupied in the $^2A_1$ state, it comprises a large Al_1(p) population (1.209) together with an Al_2(p) population of 0.731 in the $^2A_1$ state compared to the corresponding populations of Al_1(p) (0.640) and Al_2(p) (0.729) in the $^2B_1$ state. On the other hand, a doubly occupied $5a_1$ orbital (and a singly occupied $2b_1$ orbital) in the $^2B_1$ state results in noticeably large Al_1(s) population (1.859) compared to the Al_1(s) population (1.233) of the $^2A_1$ state. Likewise, the compositions of the 2e′ and 1e″ orbitals and their occupancies determine the populations of the $^2E'$ state. This state exhibits a larger Al(p) population (0.892) and a smaller Al(s) (1.648) population. On the other hand, the $^2E''$ state has a larger Al(s) population of 1.843 and a smaller Al(p) (0.707) population. As can be seen from Table 1, the dipole moment of the $^2A_1$ (C_{2v}) state is (−5.42 D), which is larger in magnitude than that of the $^2B_1$ state (−1.29 D). This is consistent with a greater charge transfer from Al to As in the former compared to the latter, as evidenced from the total Mulliken populations.

As seen from Table 2, the $Al_3As_2^+(D_{3h})$ positive ion exhibits four low-lying electronic states, namely $^3A_2'$, $^1E'$, $^3E''$, and $^1E''$. We kept the geometry of the positive ion fixed at the neutral $^2E'$ geometry, as we do not expect geometry relaxation to make a significant impact on the computed ionization energy. Furthermore, the lowest $^3A_2'$ state should retain the ideal D_{3h} structure. While the excited states of $Al_3As_2^+$ may distort, on the basis of our computed results on the neutral species, we expect the Jahn−Teller stabilization energy to be rather small. Removal of an electron from the 2e′ orbital of the $^2E'(D_{3h})$ state of the neutral Al_3As_2 results in an open-shell $2e'^2$ electronic configuration. This yields three possible electronic states, namely a $^3A_2'$ state, a $^1E'$ state, and a $^1A_1'$ state. By Hund's rule, the $^3A_2'$ state should be the lowest among these in energy consistent with our MRSDCI results in Table 2. The $^1E'$ state should be the next one in the order of energy, while the higher $^1A_1'$ state would be the second root in the C_{2v} symmetry (the first root corresponding to $^1A_1$ being $^1E'$), and was thus not computed. As seen from Table 2, the $^3A_2'$ state is the ground state of $Al_3As_2^+$, while the $^1E'$ state is 0.18 and 0.34 eV above the $^3A_2'$ state at the MRSDCI and MRSDCI+Q levels, respectively. Consequently, the positive ion would not distort in the ground state, but small geometrical distortions are anticipated in the excited states.

As seen from Table 2, the adiabatic ionization energy of Al_3As_2 is 6.84 eV at the MRSDCI level. The energy required to remove an electron from the close-shell 1e″ orbital in the $^2E'(D_{3h})$ state of the neutral cluster would be larger. This process would result in two feasible electronic states with same configuration, namely $^3E''$ and $^1E''$. As seen from Table 2, these states are 1.28 and 1.90 eV above the $^3A_2'$ ground state of $Al_3As_2^+$ at the MRSDCI level. The $^1A_1'$ state, which arises from the same configuration as the $^3A_2'$ ground state, is likely to be below the $^3E''$ and $^1E''$ states. Thus, there are at least four low-lying excited states for $Al_3As_2^+$ below 2 eV relative to the ground state.

As seen from Table 4, the $^3A_2'$ state of $Al_3As_2^+$ exhibits Al-($s^{1.539}p^{0.737}$) and As($s^{1.800}p^{3.473}$) populations, compared to the $^2E'$ state of the neutral Al_3As_2 cluster whose populations are Al-($s^{1.648}p^{0.892}$) and As($s^{1.804}p^{3.581}$). Consequently, the As(s) populations are nearly the same, while there is a significant depletion of the Al(s) population. This is fully consistent with the nature of the 2e′ orbital of the neutral species in which the Al(s) orbital makes the principal contribution. The Al(s) population decreases from 1.648 to 1.539 and 1.487 in the $^3A_2'$ and $^1E'$ states, respectively. It can be concluded that the ionization process takes place predominantly at the Al sites. This also agrees with the lower ionization potential of Al compared to As.[40] On the other hand, both As(p) and Al(p) populations decrease when an 1e″ electron is removed from the $^2E'$ state of Al_3As_2. That is, as seen from Table 4, the As(p) and Al(p) populations of the $^3E''$ and $^1E''$ states (3.318−3.325 and 0.637−0.707) are smaller than those (3.581 and 0.892, respectively) of the $^2E'$ state of Al_3As_2. This agrees with the fact that the 1e″ orbital is predominantly made of the p orbtials of the As and Al atoms. Since both As and Al sites are involved in the ionization process, higher ionization energies are required for the $^3E''$ and $^1E''$ states.

Next we consider the anion, as there is significant interest in the anion photoelectron spectroscopy of these species. As seen from Table 2, the lowest state of the $Al_3As_2^-$ anion is $^1A_1'$ with a regular trigonal bipyramid (D_{3h}) geometry. The closed-shell ground state of the $Al_3As_2^-$ anion can be justified on the basis of the low-lying states of the neutral Al_3As_2, which are $^2E'$ and $^2E''$ states. Attachment of an electron to either the open-shell 2e′ orbital in $^2E'$ or the 1e″ orbital in $^2E''$ results in the same closed-shell electronic configuration (see Table 3), yielding a $^1A_1'$ ground state for the $Al_3As_2^-$ anion. Hence the anion would not undergo Jahn−Teller distortion and remains in its ideal D_{3h} geometry. A critical comparison of the Mulliken populations of the neutral cluster and the anion reveals that the electron attachment increases the charge density of the Al(s) and As(p) orbitals. As presented in Table 4, the Al(s) and As(p) Mulliken populations of the $^1A_1'$ state of $Al_3As_2^-$ are (1.750 and 3.719) significantly larger than the corresponding values (1.648 and 3.581) of the $^2E'$ state of Al_3As_2. This is because the 2e′ orbital is principally π-bonding between the As atoms. Consequently, the As−As bond is strengthened in this state due to a filled 2e′ orbital. Thus, the As−As bond length (2.616 Å) in the $^1A_1'$ state of $Al_3As_2^-$ is contracted compared to the corresponding As−As (2.704 Å) bond length in the $^2E'$ state of Al_3As_2 at the MRSDCI level. Our computed electron affinity for Al_3As_2 is 2.33 eV at the MRSDCI level. Although it appears that there is no experimental result for the electron affinity of Al_3As_2, Xu et al.[7] have obtained the EA of In_3P_2 as 2.07 eV using anion photoelectron spectroscopy. We expect the EA of Al_3As_2 to be larger than In_3P_2 primarily due to significant participation of the As orbitals in the LUMO of Al_3As_2. Thus, our calculation exhibits the correct trend consistent with the experimental result of Xu et al.[7] on the analogous In_3P_2.

We computed the atomization energy of Al_3As_2 in a two-step sequential process. As seen from Table 2, the dissociation energy for

$$Al_3As_2(^2A_1) \rightarrow Al_3(^2A_1) + 2As(^4S)$$

is computed as 5.58 and 5.69 eV at the MRSDCI and MRSDCI+Q levels, respectively. We also computed the at-

omization energy needed to separate Al_3 into three aluminum atoms (^2P) as 3.32 and 3.58 eV at the same levels of theory. By combining the two values, the atomization energy of Al_3As_2 to form three separated Al and two As atoms is deduced as 8.90 and 9.27 eV at the MRSDCI and MRSDCI+Q levels. Because of limitations in the basis sets and electron correlation techniques, we believe that the MRSDCI+Q result of 9.27 eV should be closer to the true atomization energy of the cluster. These values confirm that the As−As and Al−As bonds play a more important role than the Al−Al bonds in the Al_3As_2 cluster.

B. Electronic States of Al_2As_3, $Al_2As_3^+$, and $Al_2As_3^-$. Table 2 shows the optimized geometries and energy separations for all of the doublet electronic states of Al_2As_3 with D_{3h} geometries. The locations of the atoms in the Al_2As_3 cluster are shown in Figure 1. In contrast to Al_3As_2, it is found that the Al_2As_3 cluster has an undistorted trigonal bipyramid (D_{3h}) geometry since the ground state is a $^2A_2''(D_{3h})$ state. The first excited $^2E''(D_{3h})$ state is 1.02 eV higher than the $^2A_2''$ state at the MRSDCI level. Another doublet state, namely $^2E'(D_{3h})$, is even higher than the $^2E''(D_{3h})$ state in energy. It is expected that both $^2E''$ and $^2E'$ states would undergo Jahn−Teller distortion, although the distortion energy is anticipated to be less than 0.4 eV. The second half of Table 1 shows our calculated results for two distorted electronic states, namely $^2A_2$ and $^2A_1$ (both C_{2v}), which are Jahn−Teller components of the $^2E''$ and $^2E'(D_{3h})$ states, respectively. Although the $^2A_2(C_{2v})$ state is lower than the corresponding $^2E''(D_{3h})$ state, due to a smaller Jahn−Teller stabilization energy of ~0.33 eV, the $^2A_2(C_{2v})$ state is still 0.69 eV higher than the undistorted $^2A_2''(D_{3h})$ state at the MRSDCI level.

The distortion in the excited states of Al_2As_3 can be illustrated by comparing the geometries of the $^2A_2(C_{2v})$ and $^2E''(D_{3h})$ states. As seen from lower parts of Tables 1 and 2, three As atoms form an equilateral triangular base in the $^2E''(D_{3h})$ state of Al_2As_3 with equilibrium As−As bond lengths of 2.457 Å. The equilateral triangular base is distorted into an isosceles triangle (the apex angle is 55.6°) in the $^2A_2(C_{2v})$ state in which the elongated isosceles sides are As_1-As_2 or As_1-As_3 (2.485 Å) and a contracted base with an As_2-As_3 bond length of 2.319 Å. The average As−As bond length of the three sides in the $^2A_2(C_{2v})$ state is 2.430 Å which is comparable to the As−As bond length (2.457 Å) in the $^2E''(D_{3h})$ state. The distance between the axial Al atoms in the $^2A_2(C_{2v})$ state is 4.865 Å, which is close to the Al−Al bond (4.828 Å) in the $^2E''(D_{3h})$ state, suggesting little distortion of the axial Al atoms. The $^2E'(D_{3h})$ state of Al_2As_3 exhibits the same features in that the equatorial atoms depart from an ideal equilateral triangular configuration into an isosceles triangular configuration, while the axial atoms are not affected.

The $1a_1'$ orbital ($1a_1$ in C_{2v}) of Al_2As_3 is predominantly $As_1(s) + As_2(s) + As_3(s)$, while the $2a_1'$ orbital ($4a_1$ in C_{2v}) is made of $Al_1(s) + Al_2(s)$. The $3a_1'$ orbital ($5a_1$ in C_{2v}) is composed of $[As_1(s) + As_2(s) + As_3(s)]$ and $[As_2(p_y) + As_3(p_y)]$. The $1e'$ orbital ($2a_1$ and $1b_2$ in C_{2v}) consists of two orthogonal degenerate linear combinations, namely $2As_1(s) - [As_2(s) + As_3(s)]$ and $[As_2(s) - As_3(s)]$, while the $2e'$ orbital ($3a_1$ and $2b_2$ in C_{2v}) is composed of $[As_2(p_z) - As_3(p_z)]$ and $[As_2(p_y) - As_3(p_y)]$. The $3e'$ orbital($6a_1$ and $3b_2$ in C_{2v}) is made up of $As_1(p_y) + As_2(p_y) + As_3(p_y)$ and $As_2(p_y) - As_3(p_y)$. The $1e''$ ($2b_1$ and $1a_2$ in C_{2v}) orbital has two orthogonal linear combinations, namely $2As_1(p_x) - [As_2(p_x) + As_3(p_x)] + [Al_1(p_y) - Al_2(p_y)$ and $[As_2(p_x) - As_3(p_x)] + [Al_1(p_z) - Al_2(p_z)$. The $1a_2''$ ($1b_1$ in C_{2v}) orbital is composed of $Al_1(s) - Al_2(s)$, while the $2a_2''$ orbital ($3b_1$ in C_{2v}) is $Al_1(p_x) + Al_2(p_x)$ combined with a nonnegligible contribution from $Al_1(s) - Al_2(s)$.

Table 3 outlines the leading configurations contributing to the electronic states of Al_2As_3. As seen from the table, all of the D_{3h} electronic states of Al_2As_3 have $(1a_1'^2 2a_1'^2 3a_1'^2 1e'^4 2e'^4 1a_2''^2)$ in common, while $(1a_1^2 2a_1^2 3a_1^2 4a_1^2 5a_1^2 1b_2^2 2b_2^2 1b_1^2\ 2b_1^2)$ is common to the $^2A_2$ and $^2A_1$ (C_{2v}) states. As evidenced from the table, the principal distinction between the low-lying $^2A_2''$ and $^2E''(D_{3h})$ electronic states originates from different electronic occupancies for the $1e''$ and $2a_2''$orbitals. The $1e''$ orbital exhibits a bond between the Al(p) and As(p), while the $2a_2''$ orbital is antibonding with respect to the two Al p and s orbitals along the x axis. The $1e''$ orbital is fully occupied in the $^2A_2''$ state, which has only an electron in $2a_2''$, resulting in shorter Al−As bonds (2.560 Å) in the $^2A_2''$ state compared to the corresponding Al−As bonds (2.800 Å) in the $^2E''$ state at the MRSDCI level. On the other hand, the $^2E''$ state has a filled $2a_2''$ orbital, but a partially filled $1e''$ orbital (three electrons) thus resulting in an elongated Al−Al (4.828 Å) bond in contrast to a shorter Al−Al bond (4.184 Å) in the $^2A_2''$ state. The $3e'$ orbital exhibits repulsive interactions among the three As atoms. Hence the $^2E'$ state, which is the only state with an electron in the $3e'$ orbital, has the longest As−As bond length (2.950 Å) among the three doublet states of the Al_2As_3 cluster. Likewise, the difference in the properties between the two distorted $^2A_2$ and $^2A_1$ states (C_{2v}) arises as a consequence of the occupancies of the $5a_1$ and $1a_2$ orbitals.

Table 4 displays the Mulliken populations on the electronic states of Al_2As_3. Most of the previous discussions for the populations of Al_3As_2 hold for Al_2As_3. All of the states of Al_2As_3 manifest Al^+As^- polarities of bonds. The As(p) contributions to the electronic states of Al_2As_3 are noticeably smaller than the corresponding values for Al_3As_2. This is consistent with the fact that the charge transferred from Al to As is shared by the three As atoms, while in the case of Al_3As_2 it is shared by two As atoms. Thus, the extent of charge transfer to each As atom is smaller in the case of Al_2As_3.

As can be inferred from Table 4, the $^2A_2''$ and $^2E''$ (D_{3h}) states are composed of $As(s^{1.876}p^{3.247})$ and $Al(s^{1.537}p^{0.939})$ and $As(s^{1.878}p^{3.223})$ and $Al(s^{1.855}p^{0.671})$ populations, respectively. A striking contrast between the two states is in the population of the Al atom, which is fully consistent with the nature of the orbitals. As indicated earlier, Al(p) participation is enhanced in the $1e''$ orbital. Although this is fully occupied in the $^2A_2''$ state, it is only partially occupied in the $^2E''$ state. This leads to a larger Al(p) population (0.939) in the $^2A_2''$ state. On the other hand, $2a_2''$ has Al(s) participation and it is fully occupied in the $^2E''$ state, but half-filled in the $^2A_2''$ state leading to a noticeably higher Al(s) population (1.855) in the $^2E''$ state compared to that of the $^2A_2''$ state (1.537). Likewise, the orbital analysis for the distorted $^2A_2$ and $^2A_1$ (C_{2v}) states explains a larger Al(s) population (1.857) in the $^2A_2$ state than that of the $^2A_1$ state (1.278), but a smaller Al(p) population (0.661) than that of the $^2A_1$ state (1.137).

The dissociation energy to dissociate Al_2As_3, into As_3 and 2Al, that is

$$Al_2As_3(^2A_2'') \rightarrow As_3(^2A_2) + 2Al(^2P)$$

is computed as 7.59 and 7.71 eV at the MRSDCI and MRSDCI+Q levels, respectively. Combing these results with the atomization energy of As_3 to yield three $As(^4S)$ atoms (5.18 eV) at the same level,[39] we obtain the atomization energy of Al_2As_3 as 12.77 and 13.12 eV at the MRSDCI MRSDCI+Q levels, respectively. Previous studies on As_2[37] and As_3[39] reveal

that the MRSDCI atomization energy for As_3 was considerably lower than the experimental value. Thus, we anticipate the MRSDCI calculations to underestimate the atomization energy of Al_2As_3. While the MRSDCI+Q technique would correct this to some extent, we anticipate the experimental atomization energy for Al_2As_3 to be larger than 13.5 eV, and this value should be treated as a lower bound.

Table 2 displays the energy separations of four low-lying electronic states of the $Al_2As_3^+(D_{3h})$ positive ion, while Table 3 presents their leading configurations. As can be inferred from Table 2, the adiabatic ionization energy to remove an electron from the $2a_2''$ HOMO of the $^2A_2''(D_{3h})$ ground state of the neutral Al_2As_3 cluster is 6.61 eV at the MRSDCI level and 6.87 eV at the MRSDCI+Q level. This process creates a closed-shell $^1A_1'$ ground state for the cation of the cluster. The energy needed to remove an electron from the $3a_1'$ orbital of the $^2A_2''$ neutral ground state is larger as expected. The removal of an electron from the $3a_1'$ orbital creates two excited electronic states, namely the $^3A_2''$ and $^1A_2''$ states. On the other hand, the removal of an electron from the $1e''$ orbital of the $^2A_2''$ state leads to the $^3E'$ and $^1E'$ excited states of which $^3E'$ would be lower. As seen from Table 2, the $^3A_2''$ and $^3E'$ states are 7.66 and 7.96 eV higher than Al_2As_3, respectively. The $^1A_2''$ state is 8.92 eV higher at the MRSDCI level from which the $^3A_2'' - {}^1A_2''$ energy splitting is obtained as 1.26 eV. The corresponding MRSDCI+Q result can be deduced from Table 2.

As can be seen from Table 4, there is a considerable decrease in the Al 3s and 3p populations as a result of the ionization process. This is consistent with the nature of the $2a_2''$ HOMO, which has Al(3p) and Al(3s) as its principal components. This is anticipated in view of the smaller ionization potential of Al compared to As, and thus ionization takes place predominantly at the axial Al sites.

The $Al_2As_3^-$ anion has a closed-shell ground $^1A_1'$ state with a regular trigonal bipyramid D_{3h} structure. Table 2 exhibits the geometry and energy of the $^1A_1'$ state of $Al_2As_3^-$. As seen from Table 2, upon electron attachment the As−As (2.495 Å) bonds are contracted, while both Al−Al (4.468 Å) and Al−As (2.658 Å) bonds are elongated in the $^1A_1'$ state of the anion compared to the corresponding bonds in the neutral $^2A_2''$ ground state. It can be inferred from Table 3 that the attached electron occupies the $2a_2''$ orbital, which is composed of the p_x orbitals of the axial Al atoms overlapping with opposite signs along the *x*-axis. Thus, the electron attachment to the $2a_2''$ orbital results in the elongation of the Al−Al axial bond. However, the electron attachment process is far more complicated in that after the attachment, there is considerable rearrangement of electronic density, as evidenced by the contractions of the As−As bonds at the base. This is also consistent with the Mulliken populations in Table 4. It can be inferred that the $^1A_1'$ state of the anion is composed of As($s^{1.853}p^{3.401}$) and Al($s^{1.739}p^{1.034}$) populations compared to the As($s^{1.876}p^{3.247}$) and Al($s^{1.537}p^{0.939}$) populations of the neutral $^2A_2''$ ground state. Thus, although initially the electron attachment takes place at the $2a_2''$ orbital, there is a significant rearrangement of electronic density. In the final picture, the As and Al atoms share the excess electron density due to the attachment process, although the Al atoms receive greater charge density compared to the As atoms.

The electron affinity (EA) of Al_2As_3 is calculated as 2.05 eV at the MRSDCI level, and it is smaller than the corresponding EA (2.33 eV) of Al_3As_2. However, we expect the two EAs to be close, and thus the theoretical value for Al_2As_3 is underestimated. Xu et al.[7] obtained the EA of In_2P_3 as 2.72 eV, while Taylor et al. obtained the EA of Ga_2P_3 as 3.03 eV. The EAs of the corresponding As clusters are expected to be smaller and thus our computed results exhibit the correct trend. The measured EAs are expected to be larger than our computed results, especially for Al_2As_3.

TABLE 5: Comparison of the Geometries and Energy Separations for the Electronic States of Al_3As_2 and Ga_3As_2 with C_{2v} Structures

	Al_3As_2		Ga_3As_2	
	$^2A_1$	$^2B_1$	$^2A_1$	$^2B_1$
$M_2-M_1-M_3$ (deg)	69.5	71.7	67.5	70.0
$X_1-M_1-X_2$ (deg)	67.9	51.1	70.8	52.6
$X_1-M_2-X_2$ (deg)	59.9	53.8	61.4	55.2
M_1-M_2 (Å)	3.641	3.902	3.702	3.986
M_2-M_3 (Å)	4.153	4.568	4.114	4.572
M_1-X_1 (Å)	2.384	2.793	2.401	2.829
M_2-X_1 (Å)	2.667	2.661	2.725	2.707
X_1-X_2 (Å)	2.663	2.410	2.782	2.507
E (CASSCF) (eV)	0.00	0.51	0.00	0.03
E (MRSDCI) (eV)	0.00	0.56	0.00	0.02
E (MRSDCI+Q) (eV)	0.00	0.47	0.00	0.005

TABLE 6: Comparison of the Geometries and Energy Separations for the Electronic States of Al_3As_2 and Ga_3As_2 with the D_{3h} Trigonal Bipyramid Structures

	state		MRSDCI				
system	C_{2v}	D_{3h}	M−M (Å)	M−X (Å)	X−X (Å)	X−M−X (deg)	*E* (eV)
Al_3As_2	$^2A_1$, $^2B_2$	$^2E'$	3.748	2.552	2.704	64.0	0.27
	$^2A_2$, $^2B_1$	$^2E''$	4.142	2.691	2.469	54.6	0.62
	$^4A_2$	$^4A_1''$	3.205	2.499	3.360	84.5	0.73
	$^4B_1$, $^4A_2$	$^4E''$	3.193	2.517	3.427	85.8	1.49
	$^4A_1$, $^4B_2$	$^4E'$	3.549	2.611	3.236	76.6	2.31
Ga_3As_2	$^2A_1$, $^2B_2$	$^2E'$	3.812	2.591	2.735	63.7	0.26
	$^2A_2$, $^2B_1$	$^2E''$	4.184	2.724	2.518	55.1	0.19
	$^4B_2$	$^4A_2'$	2.828	2.517	3.831	99.1	1.00
	$^4A_2$	$^4A_1''$	3.274	2.538	3.387	83.7	1.10
	$^4A_1$, $^4B_2$	$^4E'$	3.637	2.685	3.347	77.1	1.91
	$^4B_1$, $^4A_2$	$^4E''$	3.093	2.646	3.905	95.1	2.10

Although it appears that spectra of the Al_3As_2 and Al_2As_3 clusters are yet to be obtained, there are negative ion photoelectron spectroscopic studies of mixed indium phosphide clusters[4−5,7,8] and gallium phosphide clusters.[15,16] Mandich and co-workers[9] have obtained the photodissociation spectra of the indium phosphide clusters ranging in sizes from 5 to 14 atoms. The photoelectron spectra of $In_3P_2^-$ and $In_2P_3^-$ obtained by Xu et al.[7] reveal that each of the species exhibits two peaks. The $In_3P_2^-$ anion exhibits two peaks very close to each other and their intensities are almost same, consistent with two nearly-degenerate electronic states computed here for the isovalent Al_3As_2. The two peaks exhibited by $In_2P_3^-$ have different intensities and are well resolved compared to the $In_3P_2^-$ peaks. A possible explanation for this is that the two excited electronic states of the neutral In_2P_3 cluster, which correspond to the two peaks, are well separated in energy. This is fully consistent with the computed excited states shown in Table 7 for the isovalent Al_2As_3 and Ga_2As_3 clusters, which exhibit well-resolved excited states above their respective ground states. The photodissociation experiments[7] suggest that the In−P bonding is the dominant chemical interaction in the indium phosphide clusters ranging in sizes 5−14. This conclusion is fully supported by our computations, which show that the M−X bonds are more important than the M−M or X−X bonds in the determination of the geometries and energy separations of the M_3X_2 and M_2X_3 species.

Taylor et al.[16] have obtained the anion photoelectron spectra of $Ga_xP_y^-$ anions of varying stoichiometry up to 18 atoms. In a subsequent investigation, Taylor et al.[15] have obtained

TABLE 7: Comparison of the Geometries and Energy Separations for the Electronic States of Al_2As_3 and Ga_2As_3 with the D_{3h} Trigonal Bipyramid Structures

	state		MRSDCI				
system	C_{2v}	D_{3h}	As−As (Å)	As−Al (Å)	Al−Al (Å)	Al−As−Al (deg)	E (eV)
Al_2As_3	$^2B_1$	$^2A_2''$	2.556	2.560	4.184	109.6	0.00
	$^2A_2$, $^2B_1$	$^2E''$	2.457	2.800	4.828	119.1	1.02
	$^2A_1$, $^2B_2$	$^2E'$	2.950	2.456	3.539	92.2	1.49
	state		MRSDCI				
system	C_{2v}	D_{3h}	As−As (Å)	As−Ga (Å)	Ga−Ga (Å)	Ga−As−Ga (deg)	E (eV)
Ga_2As_3	$^2B_1$	$^2A_2''$	2.563	2.589	4.249	110.3	0.00
	$^2A_2$, $^2B_1$	$^2E''$	2.468	2.868	4.978	120.4	0.84
	$^2A_1$, $^2B_2$	$^2E'$	2.533	2.820	4.822	117.5	1.88

TABLE 8: Mulliken Populations for the Electronic States of Al_3As_2 and Ga_3As_2

						gross population								
	state		total			M_1			M_2			X		
system	C_{2v}	D_{3h}	M_1	M_2	X	s	p	d	s	p	d	s	p	d
Al_3As_2	$^2A_1$		2.547	2.623	5.605	1.233	1.209	0.105	1.822	0.731	0.070	1.815	3.615	0.175
	$^2B_1$		2.554	2.643	5.581	1.859	0.640	0.055	1.844	0.729	0.070	1.851	3.560	0.170
	$^2A_1$, $^2B_2$	$^2E'$	2.622		5.568	1.648	0.892	0.082				1.804	3.581	0.183
	$^2B_1$, $^2A_2$	$^2E''$	2.615		5.577	1.843	0.707	0.065				1.847	3.554	0.176
Ga_3As_2	$^2A_1$		2.756	2.698	5.424	1.425	1.218	0.113	1.835	0.785	0.078	1.821	3.462	0.141
	$^2B_1$		2.622	2.725	5.464	1.864	0.689	0.069	1.844	0.802	0.079	1.873	3.456	0.135
	$^2A_1$, $^2B_2$	$^2E'$	2.738		5.398	1.729	0.919	0.090				1.819	3.431	0.148
	$^2B_1$, $^2A_2$	$^2E''$	2.688		5.468	1.850	0.762	0.076				1.803	3.473	0.192

TABLE 9: Comparison of the Mulliken Populations of the Electronic States of Al_2As_3 and Ga_2As_3

					gross population					
	state		total		X			M		
system	C_{2v}	D_{3h}	X	M	s	p	d	s	p	d
Al_2As_3	$^2B_1$	$^2A_2''$	5.277	2.586	1.876	3.247	0.154	1.537	0.939	0.110
	$^2A_2$,$^2B_1$	$^2E''$	5.273	2.591	1.878	3.223	0.172	1.855	0.671	0.065
	$^2A_1$,$^2B_2$	$^2E'$	5.321	2.520	1.886	3.315	0.120	1.256	1.128	0.136
Ga_2As_3	$^2B_1$	$^2A_2''$	5.184	2.724	1.872	3.160	0.152	1.602	1.012	0.110
	$^2A_2$,$^2B_1$	$^2E''$	5.237	2.645	1.872	3.199	0.166	1.909	0.682	0.054
	$^2A_1$,$^2B_2$	$^2E'$	5.217	2.675	1.886	3.176	0.155	1.892	0.723	0.060

vibrationally resolved anion photoelectron spectra of $Ga_2P_3^-$ and a few three-atom clusters. The spectra of $Ga_2P_3^-$ and $Ga_3P_2^-$ differ in that while the spectra of the former exhibit three resolved peaks identified as X, A, and B, the latter exhibits a broad single peak, and only the ground state of the Ga_3P_2 cluster could be assigned. The $Ga_2P_3^-$ anion has been studied further with high-resolution vibrationally resolved spectra. The ground-state peak is centered at 3.14 eV, while the first excited state appears at 0.21 eV above this. On the basis of Franck−Condon simulations, the origin of the X peak was located at 3.004 eV.

IV. Comparison

Electronic States of Al_2As_3 and Ga_2As_3. The electronic states of the related Ga_2As_3 cluster have been studied using matrix-isolated ESR spectroscopy by Van Zee et al.[12] and by a comparable theoretical study[30] as well as the density functional theory[2], and it would thus be enlightening to compare the two clusters. Table 7 shows the geometries and energy separations of the doublet electronic states of the two clusters with trigonal bipyramid D_{3h} geometries. As seen from the table, there are many similarities between the two clusters. Both clusters share a $^2A_2''(D_{3h})$ ground state and a $^2E''$ first excited state.

Van Zee et al.[12] have obtained the ESR spectrum of Ga_2As_3 produced by laser-heating of GaAs crystals followed by isolation in Ar and Kr matrices. The ESR spectrum revealed a $S = {}^1/_2$ ground state for Ga_2As_3. The hyperfine pattern was found to be consistent with a structure containing three equivalent As atoms suggesting a regular trigonal bipyramidal structure. From the observed hyperfine pattern of Ga_2As_3, Van Zee et al.[12] inferred that the unpaired electron resides on an orbital, which is entirely on the two axial gallium atoms. All of these features are in complete accord with our computations on the isovalent Al_2As_3 cluster, which is predicted to have a $^2A_2''$ ground state with an ideal D_{3h} structure. As discussed earlier, in the ground state of Al_2As_3, the singly occupied $2a_2''$ HOMO is composed of $Al_1(p_x) + Al_2(p_x)$ with a nonnegligible contribution from Al_1-(s) − Al_2(s). For the case of Ga_2As_3, the unpaired $2a_2''$ electron is localized on the two axial Ga atoms. Thus, our theoretical calculations fully support the experimental results of Van Zee et al.[12]

Table 7 compares the geometries and energy separations of the electronic states of the two clusters. As seen from the table, both clusters have almost the same As−As bond lengths (∼2.56 Å) and M−As−M bond angles (∼110°) in their ground states, implying that the As−As bonds are quite similar. It can be seen from Table 7 that the actual As−As bond lengths in the $^2A_2''$ ground state are 2.556 and 2.563 Å. As seen from Table 7, although the first excited states of the two clusters are similar, the second excited states differ primarily due to the differences in the characteristics of the metal−metal bonding.

Electronic States of Al_3As_2 and Ga_3As_2. The isovalent Ga_3As_2 cluster has previously been studied theoretically,[2,30] and thus it would be interesting to compare the properties of the two clusters. Table 5 shows the optimized geometries and energy

separations for the distorted $^2A_1$ and $^2B_1$ electronic states of these clusters with the C_{2v} geometries, while Table 6 compares the equilibrium geometries and energy separations of the undistorted D_{3h} states with trigonal bipyramid structures. As seen from the tables, all these species have the $^2E'$ and $^2E''$ states as the lowest-lying states in D_{3h} symmetry; both states undergo Jahn−Teller distortion resulting in distorted states. As seen from Table 5, both clusters possess the same distorted $^2A_1$ ground state with C_{2v} geometries. We have already considered Jahn−Teller distortion extensively in these clusters. As inferred from Table 5, the As−As distances in the $^2A_1(C_{2v})$ ground state are 2.663 and 2.782 Å for Al_3As_2 and Ga_3As_2, respectively. The values are comparable to the corresponding As−As bonds in the undistorted $^2E'$ state, viz., 2.719 and 2.762 Å, suggesting little changes to the two As atoms due to Jahn−Teller distortion. However, the three metal atoms depart from their equilateral M_3 base position in the D_{3h} states by Jahn−Teller distortion resulting in contracted M_1-M_2 (or M_1-M_3) and elongated M_2-M_3 bonds.

The As−As bond lengths in the corresponding states of Al_3As_2 and Ga_3As_2 are quite similar. For example, the shortest As−As bond distances in the distorted $^2B_1$ state are not too far from the diatomic As_2[37] distance. The metal−metal bond lengths in the ground states of M_3 are 2.521 and 2.58 Å[38,40] for M = Al and Ga respectively, which are much shorter compared to the Al−Al (3.5−4.1 Å) and Ga−Ga (3.7−4.1 Å) bonds in the ground states of M_3As_2. Evidently, the M−M bonds in M_3As_2 are dramatically weakened by the interaction between the metal and As atoms.

As evidenced from both Tables 5 and 6, there is a significant difference between Al_3As_2 and Ga_3As_2 with regard to the $^2B_1-{}^2A_1$ and $^2E''-{}^2E'$ energy separations. Whereas the $^2B_1(^2E'')$ and $^2A_1(^2E')$ electronic states are virtually degenerate for Ga_3As_2, this is not the case for Al_3As_2. As seen from Table 5, the $^2B_1-{}^2A_1(C_{2v})$ energy separations are 0.56 and 0.47 eV at the MRSDCI and MRSDCI+Q levels, respectively, for Al_3As_2, while the corresponding values are 0.02 and 0.005 eV for Ga_3As_2 at the same levels of theory. As seen from Table 6, a similar trend is seen for the $^2E''-{}^2E'$ energy separations, and in fact at the MRSDCI level of theory, the $^2E''$ state is 0.07 eV lower than $^2E'$ for Ga_3As_2. This requires explanation in view of the fact that Al and Ga are similar in many other ways. This apparent anomaly can be rationalized on the basis of the bonding and Mulliken populations of the two clusters. As evidenced from Table 8, while the metal and As Mulliken populations are so similar for the $^2B_1$ state, the corresponding populations for the $^2A_1$ state differ substantially for the Ga and Al clusters. The $Al_1(3s)$ population (1.233) is substantially reduced compared to the $Ga_1(4s)$ population of 1.425 in the $^2B_1$ state, and the As(4p) population in Al_3As_2 increases to 3.615 compared to 3.462 in Ga_3As_2. This suggests increased charge transfer from Al(3s) to As(4p) for the $^2A_1$ state of Al_3As_2 resulting in enhanced ionicity in the case of Al_3As_2 cluster compared to Ga_3As_2. Consequently, a larger charge transfer stabilizes the $^2A_1$ state to a greater extent for Al_3As_2 compared to Ga_3As_2.

Although all of the quartet states of M_3As_2 are much higher than the ground state due to occupied antibonding orbitals, there exists notable differences in the energy order. As seen from Table 6, the three quartet states, namely $^4A_2''$, $^4E''$, and $^4E'$ of Al_3As_2 are 0.73, 1.49, and 2.31 eV higher than the ground state, respectively. But the quartet states of Ga_3As_2 are more closely spaced in that the $^4A_2'$, $^4A_1''$, $^4E'$, and $^4E''$ states are 1.00, 1.10, 1.91, and 2.10 above the ground state of Ga_3As_2. This is primarily due to the fact[41] that the *J*-weighted $^4S-{}^2D$ separation for As is 10 790 cm^{-1}, and it is lower than the corresponding separation of 11 371 cm^{-1} for P.

Acknowledgment. This research was support by the U.S. National Science Foundation under grant CHE9814056. P.Y.F. thanks Dr. Zou, the ex-director of Shanghai Metallurgy Institute, for facilitating this cooperation.

References and Notes

(1) O'Brien, S. C.; Liu, Y.; Zhang, Q. L.; Heath, J. R.; Tittel, F. K.; Curl, R. F.; Smalley, R. E. *J. Chem. Phys*. **1986**, *84*, 4074. Liu, Y.; Zhang, L.; Tittel, F. K.; Curl, R. F.; Smalley, R. E. *J. Chem. Phys*. **1986**, *85*, 7434.

(2) Wang, L.; Chibante, L. P. F.; Tittel, F. K.; Curl, R. F.; Smalley, R. E. *Chem. Phys. Lett*. **1990**, *172*, 335. Lou, L.; Wang, L.; Chibante, P. F.; Laaksonen, R. T.; Nordlander, P.; Smalley, R. E. *J. Chem. Phys*. **1991**, *94*, 8015. Lou, L.; Nordlander, P.; Smalley, R. E. *J. Chem. Phys*. **1992**, *97*, 1858.

(3) Jin, C.; Taylor, K.; Conciecao, J.; Smalley, R. E. *Chem. Phys. Lett*. **1990**, *175*, 17.

(4) Arnold, C. C.; Neumark, D. M. *J. Chem. Phys*. **1994**, *99*, 3353.

(5) Arnold, C. C.; Neumark, D. M. *J. Chem. Phys*. **1994**, *100*, 1797. Arnold, C. C.; Neumark, D. M. *Can. J. Phys*. **1994**, *72*, 1322.

(6) Bernstein, E. R. Atomic and Molecular Clusters. *Stud. Phys. Theor. Chem.* **1990**, *68*, 69.

(7) Xu, C.; deBeer, E.; Arnold, D. W.; Neumark, D. M. *J. Chem. Phys*. **1994**, *101*, 5406.

(8) Burton, G. R.; Xu, C.; Arnold, C. C.; Neumark, D. M. *J. Chem. Phys*. **1996**, *104*, 2757.

(9) Kolenbrander, K. D.; Mandich, M. L. *J. Chem. Phys.* **1990**, *92*, 4759. Rinnen, K.-D.; Kolenbrander, K. D.; DeSantolo, A. M.; Mandich, M. L. *J. Chem. Phys*. 1992, **96**, 4088.

(10) Rasanen, M.; Heimbrook, L. A.; Schwartz, G. P.; Bondybey, V. E. *J. Chem. Phys.* **1986**, *85*, 86.

(11) Li, S.; Van Zee, R. J.; Weltner, W. Jr. *J. Phys. Chem.* **1993**, *97*, 11393; *J. Chem. Phys*. **1994**, *100*, 7079.

(12) Van Zee, R. J.; Li, S.; Weltner, W. Jr. *J. Chem. Phys*. **1993**, *98*, 4335.

(13) Xu, C.; Burton, G. R.; Taylor, T. R.; Neumark, D. M. *J. Chem. Phys* **1997**, *107*, 3428.

(14) Xu, C.; Taylor, T. R.; Burton, G. R.; Neumark, D. M. *J. Chem. Phys* **1998**, *108*, 1395.

(15) Taylor, T. R.; Asmis, K. R.; Gomez, H.; Neumark, D. M. *Eur. Phys. J.*, in press. Asmis, K. R.; Taylor, T. R.; Neumark, D. M. *Chem. Phys. Lett*. **1999**, *308*, 347. Taylor, T. R.; Neumark, D. M., private communication, 1999

(16) Taylor, T. R.; Asmis, K. R.; Xu, C.; Neumark, D. M. *Chem. Phys. Lett.* **1998**, *297*, 133.

(17) Lou, L.; Wang, L.; Chibante, L. P. F.; Laaksonen, R. T.; NordLander, P.; Smalley, R. E. *J. Chem. Phys*. **1991**, *94*, 8015.

(18) Lou, L.; NordLander, P.; Smalley, R. E. *J. Chem. Phys*. **1992**, *97*, 1858.

(19) Wheeler, R. G.; LaiHing, K.; Wilson, W. L.; Duncan, M. A. *J. Chem. Phys*. **1988**, *88*, 2831.

(20) LaiHing, K.; Chen, P. Y.; Duncan, M. A. *J. Phys. Chem.* **1987**, *91*, 6521.

(21) Bishop, M. B.; LaiHing, K.; Cheng, P. Y.; Peshcke, M.; Duncan, M. A. *J. Phys. Chem.* **1989**, *93*, 1566.

(22) Willey, K. F.; LaiHing, K.; Taylor, T. G.; Duncan, M. A. *J. Phys. Chem.* **1993**, *97*, 7435.

(23) Micic, O. I.; Sprague, J. R.; Curtis, C. J.; Jones, K. M.; Machol, J. L.; Nozik, A. J.; Giessen, B.; Flugel, B.; Mohs, G.; Peyghambarian, N. *J. Phys. Chem.* **1995**, **99**, 7754.

(24) MacDougall, J. E.; Eckert, H.; Stucky, G. D.; Herron, N.; Wang, Y.; Moller, K.; Bein, T.; Cox, D. *J. Am. Chem. Soc*. **1989**, *111*, 8006.

(25) Andreoni, W. *Phys. Rev. B* **1992**, *45*, 4203.

(26) Balasubramanian, K. *Chem. Phys. Lett*. **1988**, *159*, 71.

(27) Balasubramanian, K. *Chem. Rev.* **1990**, *90*, 93.

(28) Balasubramanian, K. *Chem. Rev.* **1989**, *89*, 1801.

(29) Meier, U.; Peyerimhoff, S. D.; Grien, F. *Chem. Phys.* **1991**, *150*, 331.

(30) Liao, M. Z.; Dai, D.; Balasubramanian, K. *Chem. Phys. Lett*. **1995**, *239*, 124.

(31) Feng P. Y.; Balasubramanian, K. *Chem. Phys. Lett.* **1997**, *265*, 547.

(32) Feng P.Y.; Balasubramanian, K. *Chem. Phys. Lett*. **1999**, *301*, 458.

(33) Pacios, L. F.; Christiansen, P. A. *J. Chem. Phys.* **1985**, *82*, 2664. Hurely, M. M.; Pacios, L. F.; Christiansen, P. A.; Ross, R. B.; Ermler, W. C. *J. Chem. Phys.* **1986**. *84*, 6840.

(34) Schmidt, M. W.; Baldridge, K. K.; Boatz, J. A.; Elbert, S. T.; Gorden, M. S.; Jensen, J. H.; Koseki, S.; Matsunaga, N.; Nguyen, K. A.; Su, S. J.; Windus, Dupuis, M.; Montgomery, J. A. *J. Comput. Chem*. **1993**. *14,* 1347.

(35) Balasubramanian, K. *Chem. Phys. Lett.* **1986**, *127*, 324.

(36) The major authors of ALHEMY II are: Liu, B.; Lengsfield, B.; Yoshimine, M.

(37) Balasubramanian, K. *J. Mol. Spectrosc*. **1987**, *121*, 465.

(38) Basch, H. *Chem. Phys. Lett.* **1987**, *136*, 289.

(39) Balasubramanian, K.; Sumathi, K.; Dingguo, D. *J. Chem. Phys.* **1991**. **95**, 3494.

(40) Balasubramanian, K.; Feng P. Y. *Chem. Phys. Lett.* **1988**, *146*, 155.

(41) Huber, K. P.; Herzberg, G. *Constants of Diatomic Molecules*; Van Nostrand Reinhold: New York, 1979.

(42) Moore, C. E. *Tables of Atomic Energy Levels*; U.S. National Institute of Stands and Technology, Circular 467, 1971; Vol. I−III.